ACS Chemical Neuroscience

Research Article

pubs.acs.org/chemneuro

Optimized Real-Time Monitoring of Glutathione Redox Status in Single Pyramidal Neurons in Organotypic Hippocampal Slices during Oxygen–Glucose Deprivation and Reperfusion

Bocheng Yin,[†] Germán Barrionuevo,[‡] and Stephen G. Weber*[,†]

[†]Department of Chemistry, University of Pittsburgh, Pittsburgh, Pennsylvania 15260, United States

[‡]Department of Neuroscience, University of Pittsburgh, Pittsburgh, Pennsylvania 15260, United States

Supporting Information

ABSTRACT: A redox-sensitive Grx1–roGFP2 fusion protein was introduced by transfection into single pyramidal neurons in the CA1 subfield of organotypic hippocampal slice cultures (OHSCs). We assessed changes in the GSH system in neuronal cytoplasm and mitochondria during oxygen–glucose deprivation and reperfusion (OGD/RP), an *in vitro* model of stroke. Pyramidal cells in a narrow range of depths below the surface of the OHSC were transfected by gene gun or single-cell electroporation with cyto- or mito-Grx1–roGFP2. To mimic the conditions of acute stroke, we developed an optimized superfusion system with the capability of rapid and reproducible exchange of the solution bathing the OHSCs. Measurements of pO_2 as a function of tissue depth show that in the region containing the transfected cells, the pO_2 is well-controlled. We also found that the pO_2 changes on the same time scale as changes in intracranial pressure, cerebral blood flow, and pO_2 during acute stroke. Determining the reduction potential, E_{GSH}, from the ratiometric fluorescence signal requires an absolute intensity measurement during calibration of the Grx1–roGFP2. Using the signal from cotransfected tdTomato as an internal standard during calibration improves quantitative measurements of Grx1–roGFP2 redox status and allows E_{GSH} to be determined. E_{GSH} becomes more reducing during OGD and more oxidizing during RP in mitochondria while changes in cytoplasm are not significant compared with controls.

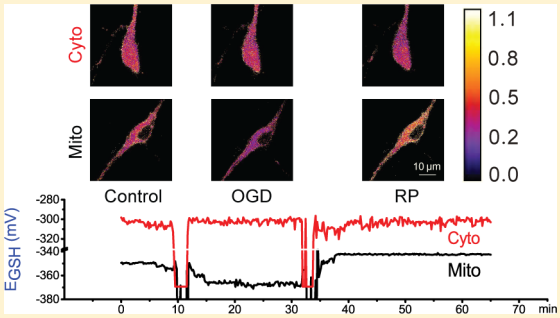

KEYWORDS: *Glutathione redox, oxygen–glucose deprivation and reperfusion, Grx1–roGFP2, organotypic hippocampal slice cultures*

Neuronal damage in stroke,[1−3] trauma,[4−6] hypoxia,[7] Alzheimer's disease,[8−12] Huntington's disease,[13,14] psychiatric conditions,[15−17] and other diseases[3,18−20] is in part caused by oxidative stress due to excessive production of reactive oxygen species (ROS).[21−23] Because ROS also play a role in cell signaling,[24−29] neurons and glial cells are endowed with mechanisms for maintaining ROS homeostasis including the glutathione–glutathione disulfide couple (GSH/GSSG) and the thioredoxin system. The GSH system becomes more oxidizing in brain with aging due to the decreasing production and increasing consumption of GSH.[30] The most obvious role of GSH in brain cells is to remove excess H_2O_2 and other ROS created acutely during short-term biological processes.[31] A more sustained activity of GSH is the promotion of cell survival by participating in beneficial enzymatically catalyzed reactions[30,32] like those of glutathione peroxidases (GPxs) and glutathione S-transferases (GSTs), while inhibiting lethal enzymes, like lipoxygenases (LOXs), which are correlated with neuron death.[30] GSH helps to detoxify excess methyl glyoxal (MG) and advanced glycation end-products, which can alter the structure and activity of a variety of proteins, leading to neuronal dysfunction and death.[30] Increasing intracellular GSH concentration and maintaining a more reduced GSH/GSSH system appears to be a promising therapeutic approach in Alzheimer's disease,[33] Parkinson's disease,[34] and autism.[35] Hypoxia/ischemia (HI) episodes, such as those that occur during stroke, disrupt ROS homeostasis leading to short-term effects in cellular function and longer-term changes that ultimately cause cell death.[36−38]

Several approaches exist for measuring ROS in real time including those based on voltammetry[39−42] and fluorescence microscopy based on fluorogenic small molecule probes.[43−46] However, there are no small-molecule redox-sensitive fluorophores that respond to the GSH system. Thus, it is noteworthy that several groups have developed the ability to measure its status in real time. Specifically, different redox protein-based sensors were developed simultaneously by the Winther (rxYFP[47]) and the Tsien and Remington groups (roGFP[48,49]). The sensor response kinetics were relatively slow, and they were oxidized to varying degrees by a variety of oxidizing agents.[48] Altering the electrostatic environment of the active disulfide by engineering amino acid substitutions in the

Received: July 6, 2015
Accepted: August 20, 2015
Published: August 20, 2015

DOI: 10.1021/acschemneuro.5b00186
ACS Chem. Neurosci. 2015, 6, 1838−1848

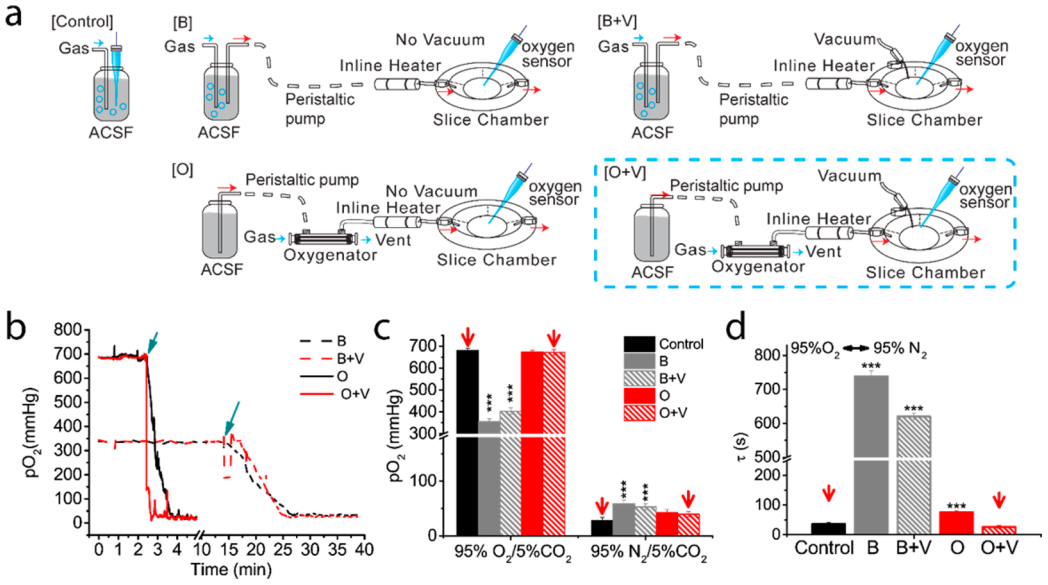

Figure 1. Measurements of pO_2 in different superfusion systems in the absence of an OHSC. (a) The conical probe represents the oxygen electrode. In "Control", oxygen is directly measured in a reservoir with solution continuously bubbled with gas. In the remaining four panels, pO_2 is measured in the slice chamber. The solution is driven by a peristaltic pump. Solutions are switched in all cases by pumping from a second reservoir containing the new solution. In the scheme labeled "[B]", solution from a reservoir being bubbled with gas is flowing continuously. [B+V] represents the same conditions as [B], but in addition, when the solution is switched to a new solution, existing solution is removed from the chamber by vacuum suction. In [O], solution is gassed by an oxygenator. [O+V] is the same conditions as [O] except that solution is removed by suction when the switch is made. (b) Continuous measurement of pO_2 in the slice chamber during superfusion with the four arrangements described in panel a. Note the break and the change in the time scale. The solution is switched from 95% O_2/5% CO_2 to 95% N_2/5% CO_2 (indicated by the green arrow point). τ is the time from the solution switch to the onset of a new steady-state pO_2. (c) Steady-state pO_2 measured in control and the four superfusion systems described in panel a. Arrows indicate control and system [O+V]. (d) τ from the five systems described in panel a. One-way ANOVA with post hoc test (***$p < 0.001$, $n = 6$, in panels c and d).

region of the modified GFPs increased the rate of reaction of the sensors with GSH/GSSG.[49,50] Meyer et al.[51] discovered that roGFP's reaction with GSH/GSSG was catalyzed by endogenous glutaredoxin (Grx). Gutscher et al.[52] made a chimeric protein, Grx1−roGFP2 that responded rapidly to cytosolic changes in GSH/GSSG status. In addition, they determined that the isolated Grx1−roGFP2 was not oxidized by cystine, hydroxyethyl disulfide, or H_2O_2 and was not reduced by ascorbate, cysteine, or the thioredoxin system (thioredoxin, thioredoxin reductase, and NADPH). Thus, this sensor is quite selective for the glutathione redox couple. Another advantage of these sensor proteins is that their pH dependence is identical to that of the GSH/GSSG redox couple. Thus, the quantity $[GSH]^2/[GSSG]$ can be determined without knowledge of the pH after proper sensor calibration *in situ*. However, knowledge of the equilibrium redox potential of the GSH system, E_{GSH}, requires knowledge of (or an assumption about) the local pH.[52]

While these sensors have illuminated redox events in a variety of types of cells, they have not been used extensively in mammalian central nervous system (CNS) tissue. Using primary cultures of hippocampal neurons from rats, Funke[53] carefully compared the response of roGFP1 against a widely used small molecule sensor hydroethidine. These investigators showed a "proof of principle" that roGFP1 would respond to exogenous peroxide application to an organotypic hippocampal slice culture (OHSC). However, there was no attempt to infer biological information from the observed response. Grosser et al., using roGFP1, studied OHSCs from a Rett syndrome mouse model.[54] They found that cytoplasmic GSH status was more oxidized in the Rett syndrome hippocampus than in controls. Hasel et al.[55] contrasted dendritic and somatic responses of Grx1−roGFP2 to stressors in cultured neurons. The dendritic regions were more oxidized compared with the somatic regions under resting conditions. Under stress, the dendritic regions changed more dramatically than somatic regions. More recently, Breckwoldt et al.[56] created a mouse that expressed Grx1−roGFP2 in neuronal mitochondria. They used this model with multiparametric imaging to investigate redox and size changes in mitochondria in explants of neuromuscular junctions and in lesioned spinal axons *in vivo*.

Thus, far, the few investigations of the GSH system's status in CNS tissue have employed roGFP1 rather than the more rapidly responding and selective Grx1−roGFP2 sensor. There are no reports that we are aware of that use the latter sensor to determine redox events in cortical CNS tissue. Here we describe a method for investigating redox events during oxygen−glucose deprivation and reperfusion (OGD/RP) in the CA1 subfield of OHSCs[57] using Grx1−roGFP2. OHSCs subjected to OGD/RP are a useful *in vitro* model of HI.[58−60] We have validated that the transfection occurs within a narrow range of depths into the culture and that the pO_2 during OGD and RP are reproducible in this range of depths. We have also improved the standard superfusion system so that changes in pO_2 occur on the same time scale as they do in *in vivo* models of stroke. In addition, calibration of Grx1−roGFP2 is improved by cotransfecting with the redox-insensitive tdTomato. Fluorescence from tdTomato provides a reference during calibration when absolute (not ratiometric) intensities from the Grx1−roGFP2 sensor are needed to report well-defined redox parameters (e.g., degree of oxidation of the sensor (OxD), E_{GSH}) as opposed to the measured ratiometric response

DOI: 10.1021/acschemneuro.5b00186
ACS Chem. Neurosci. 2015, 6, 1838−1848

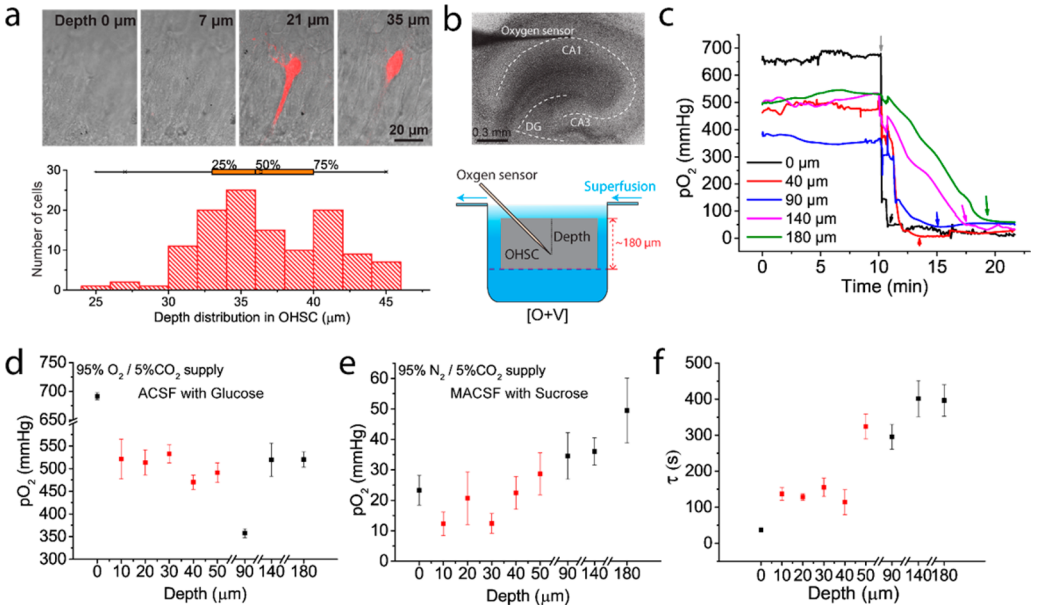

Figure 2. pO_2 varies with depth inside OHSC in the optimized superfusion system. (a, top) Confocal "slices" at different depths (Video S-1, Supporting Information). (a, bottom) Transfected cells are mostly located 30−45 μm below the surface of the culture (n = 121 cultures). (b) pO_2 measured in OHSCs with superfusion system [O+V]. (c) pO_2 profile at different depths in the OHSC before and after superfusate was switched from 95% O_2/5% CO_2 to 95% N_2/5% CO_2. Gray arrow indicates the switching time. The value of τ is the time difference between the gray arrow and the second arrow (labeled with the same color as the correspondings trace). (d, e) pO_2 in OHSC vs depth in OHSCs for 95% O_2/5% CO_2 and 95% N_2/5% CO_2. Red symbols are in the range of depths where we transfect cells and make measurements. (f) τ measured at different depths inside the OHSC. Error bars from six individual tests in panels d−f.

only.[53−56] Using this optimized approach, we have found that the GSH system changes rapidly and significantly during OGD/RP in mitochondria but not in cytoplasm of CA1 neurons.

RESULTS AND DISCUSSION

Control of pO_2 in OHSCs. The conventional method of slice oxygenation relies on bubbling the superfusion solution, ACSF containing 10 mM D-glucose, with 95% O_2/5% CO_2 and delivering it to the slice chamber with a peristaltic pump (method [B], Figure 1a). OGD is initiated by changing the superfusion solution to ACSF containing 10 mM sucrose in place of the glucose (modified ACSF, MACSF) saturated with 95% N_2/5% CO_2 (see Methods for the details of the solution compositions). We measured changes in pO_2 within the cell dish with no slice culture using four different superfusion systems (Figure 1). In methods [B] and [B+V], the tube leading to the pump was manually switched from one reservoir to another to change conditions, and the temperature of the incoming fluid was controlled online. In method [B], the solution flows continuously while it is bubbled with gas in its reservoir. [B+V] adds a step: the fluid in the slice chamber is removed by vacuum at the time the solutions are switched. In [O] and [O+V], the solution is gassed by an online oxygenator placed near the chamber. The oxygenator uses microfluidic channels with a thin, gas-permeable membrane to introduce oxygen to the solution as it passes through the device. In [O +V], the solution in the chamber is removed by vacuum when the gas supply and the source reservoir are switched. We investigated the four superfusion systems and compared them with the control (Figure 1a−d). Clearly system [O+V] (highlighted in the blue box, Figure 1a) maintained the desired oxygen level in the slice chamber (Figure 1c). Furthermore, the transition time for complete solution exchange also was dramatically shortened to less than 30 s using the system [O +V]. In contrast, the other three superfusion systems showed significant differences from the control (Figure 1d). The optimization of the superfusion system to ensure efficient exchange of solutions for OGD/RP experiments is described in Methods and Supporting Information.

By controlling the transfection conditions (see Methods and Supporting Information), we were able to target pyramidal cells localized within a relatively narrow range of distances below the surface of the OHSC. Half of the transfected cells are confined to 33−40 μm below the surface shown in Figure 2a. Thus, we measured pO_2 at various depths within the cultured slice,[61] Figure 2b, as solution conditions were changed by using [O+V] (Figure 2c). Note that the changes in pO_2 in the OHSC at depths less than about 50 μm occurs rapidly. The steady-state pO_2 during superfusion with ACSF saturated with 95% O_2/5% CO_2 (Figure 2d) ranges from 691 ± 6 mmHg at the top surface to a minimum of 358 ± 10 mmHg in the middle and 520 ± 17 mmHg at the bottom surface. This is consistent with two facts. One is that oxygen takes time to diffuse into the OHSC and it is consumed on the way.[62] The other is that the culture is maintained with the interface method, so the lower surface of the culture is exposed to the medium underneath, which is in equilibrium with air. The pO_2 distribution during superfusion with MACSF saturated with 95% N_2/5% CO_2 and transition times (τ) show similar trends (Figure 2e, f) indicating that the depth is a significant factor in controlling tissue oxygenation.

Because we use a rapidly responding roGFP-based sensor, it is instructive to observe its response during OGD/RP under the four superfusion conditions described above. Pyramidal neurons in the CA1 region of OHSCs were transfected by gene gun with mito-Grx1−roGFP2. Individual transfected pyramidal neurons were observed for 1 h during an OGD/RP protocol: 10 min ACSF, 95/5 O_2/CO_2; 20 min MACSF, 95/5 N_2/CO_2;

DOI: 10.1021/acschemneuro.5b00186
ACS Chem. Neurosci. 2015, 6, 1838−1848

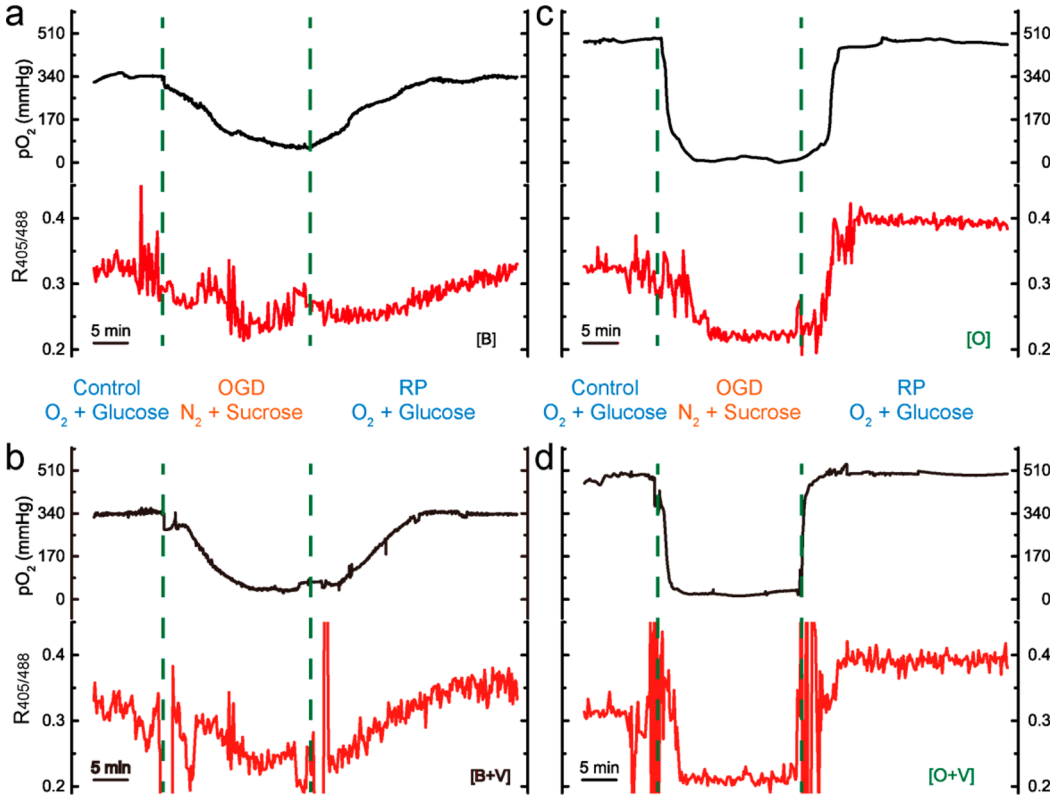

Figure 3. mito-Grx1−roGFP2 signal tracks pO_2 changes during OGD/RP. Each of the four quadrants represents a superfusion method: (a) method [B]; (b) method [B+V]; (c) method [O]; (d) method [O+V]. In each quadrant, there are traces of pO_2 (top) and the mito-Grx1−roGFP2 ratiometric signal, $R_{405/488}$ (bottom), measured simultaneously in OHSCs versus time. "Control", "OGD", and "RP" correspond to superfusion with ACSF saturated with 95% O_2/5% CO_2, MACF saturated with 95% N_2/5% CO_2, and ACSF with 95% O_2/5% CO_2, respectively. Each trace is representative of three separate experiments. $R_{405/488}(t)$ reflects the redox status of the GSH system, which changes with extracellular pO_2. The [O+V] configuration significantly improved gas exchange within the OHSC thereby decreasing the response time of the Grx1−roGFP2.

30 min ACSF, 95/5 O_2/CO_2. Figure 3a−d shows that the Grx1−roGFP2 signal changes on the same time scale as that of pO_2 in the four superfusion systems. Note that in all cases described here and below when oxygen is replaced by nitrogen, glucose is replaced by sucrose in the superfusion solution to create OGD. The solution composition is changed back to that containing oxygen and glucose to create RP.

The time-dependence of the pO_2 profile should reflect that seen for *in vivo* models of stroke,[63] which is minutes.[64] Nakai et al. reported that pO_2 and cerebral blood flow (CBF) fell "immediately" after induction of focal ischemia.[65] More quantitatively, Peters et al. found changes in cortical CBF within 5 min (the shortest time measured) after induction of focal ischemia and again at reperfusion.[66] Okada reported in transient global ischemia that CBF changes at the induction of ischemia and also at reperfusion within 1 min.[67] Westermaier et al. saw local cortical blood flow drop in 1 min while pO_2 dropped in 2−3 min in a subarachnoid hemorrhage model.[68] Prunell determined, also in a subarachnoid hemorrhage model, that CBF dropped in 40 s while pO_2 reached a minimum in 1.5−2 min.[69] Returning to Figure 2 and noting that the condition described in Figure 2d corresponds to conditions before (control) and after (reperfusion) OGD, while that in Figure 2e corresponds to OGD, we see clearly that the pO_2 is well controlled in a narrow range of values before, during, and after OGD at the depth of the OHSC where the transfected cells are located. No significant differences in pO_2 are found in the 10−50 μm depth range ($p > 0.05$, $n = 6$, one-way ANOVA, Figure 2d,e). The response of *tissue* pO_2 in the same range of depths occurs in about 2 min or less. Values of τ are not statistically different in this range of depths ($p > 0.05$, $n = 6$, one-way ANOVA, Figure 2f). Therefore, the [O+V] superfusion system is able to provide reproducible steady-state oxygenation to pyramidal cells within the range of 10 to 50 μm below the surface of the OHSC during OGD/RP experiments. The pO_2 changes on the same time scale as previously reported for *in vivo* models of stroke (cited above).

tdTomato Used As an Internal Standard Corrects for Shape Changes in Pyramidal Cells during Calibration of the Grx1−roGFP2 Signal. In OHSCs that have not been subjected to OGD/RP, there are very small or no changes in cell size during exposure to the calibrants (Figure 4a). However, during calibration after OGD/RP, there are significant changes in cell size (Figure 4b and Figure S-5b in Supporting Information). roGFP2 is ratiometric, so cell size does not change the measured ratio. However, to determine the degree of oxidation of the sensor and redox potentials of the sensor and the GSH/GSSG system, we must measure the *absolute* intensities of Grx1−roGFP2 excited at 488 nm (during calibration) in its fully oxidized form, I_{488}^{Ox}, and in its fully reduced form, I_{488}^{Red}. These intensities are influenced by changes in cell size (Figure 4d). We have found that the fluorescence emission intensity of tdTomato[70] is not sensitive to the calibrants H_2O_2 or dithiothreitol (DTT) (Figure 4a,c; Figure S-5a,c and Video S-3 in Supporting Information). In the following discussion, it will be helpful to define some terms. We excite tdTomato at 561 nm; thus we refer to the intensity of the emission from that excitation as I_{561}. We then define ratios of

DOI: 10.1021/acschemneuro.5b00186
ACS Chem. Neurosci. 2015, 6, 1838−1848

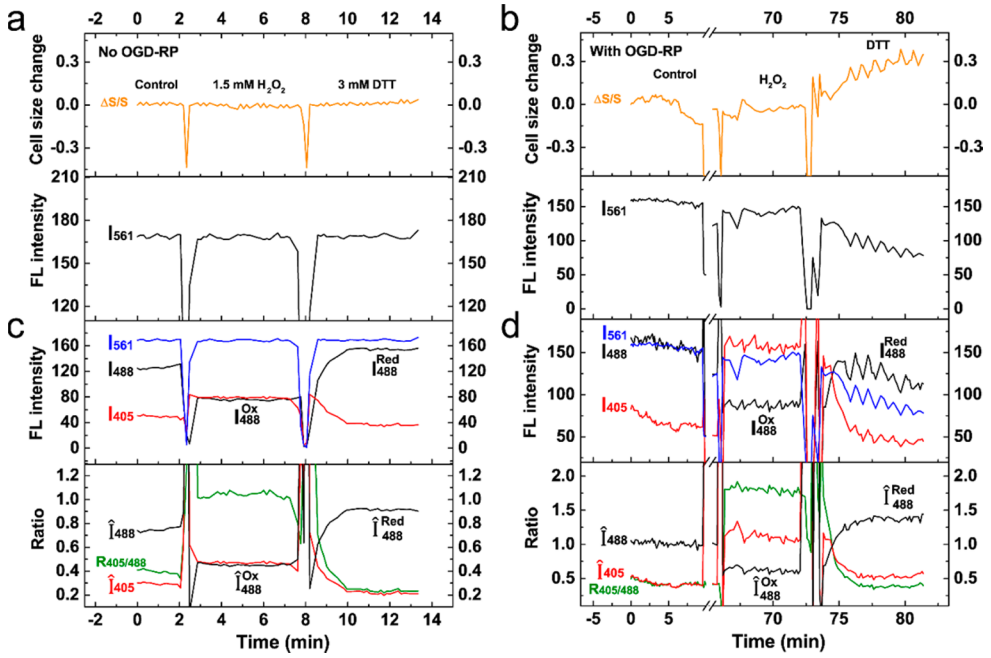

Figure 4. tdTomato corrects for changes in cell morphology allowing for stable signal during calibration. Fluorescence emission of tdTomato (excited at 561 nm) and Grx1−roGFP2 (excited at 405 and 488 nm) recorded from cytoplasm of a CA1 pyramidal cell in an OHSC. (a, top) With no OGD/RP, the cell area does not change during exposure to calibrants H_2O_2 and DTT. (a, bottom) tdTomato fluorescence emission is not sensitive to H_2O_2 and DTT. (b, top) With OGD/RP, $\Delta S/S$, cell size, changes dramatically, does not reach a steady state, and oscillates. (b, bottom) Fluorescence signal from tdTomato is inversely correlated with changes in cell size during calibration. (c) The absolute intensities (top) and ratios (bottom) from the three channels during sequential exposure to ACSF, H_2O_2, and DTT with no OGD/RP. No differences in trends are observed when comparing the absolute intensities (top panel of c) and ratios (bottom). (d) tdTomato calibration is necessary for calibration after OGD/RP with superfusion system [O+V] as described in Figure 1. Note the difference in I_{405} vs $\hat{I}_{405}$ and I_{488} vs $\hat{I}_{488}$ during exposure to DTT. Fluorescence traces prior to OGD/RP (control) and during calibration post-OGD/RP with H_2O_2 and DTT are shown (note the break in the time axis). The value of $\hat{I}_{488}^{Red}$ (bottom of panel d) is significantly more stable than the I_{488}^{Red} fluorescent signal (d, top). The confounding effects of OGD-induced cell size changes on I_{488} are corrected by I_{561}. $\hat{I}_{488}^{Ox}$ and $\hat{I}_{488}^{Red}$ are used to calculate the degree of oxidation of Grx1−roGFP2, OxD_{roGFP2} (see Supporting Information for more details). The curves shown here are representative examples from five sets of measurements on five different OHSCs.

I_{488}^{Ox} and I_{488}^{Red} to I_{561} as $\hat{I}_{488}^{Ox}$ and $\hat{I}_{488}^{Red}$ respectively. More generally, the ratio of the intensity from exciting roGFP2 at 488 nm to the intensity from 561 nm excitation of tdTomato is $\hat{I}_{488}$. See Supporting Information for more discussion of these terms and their relationships. Notably, Figure 4b and Figure S-5b show that I_{561} is inversely correlated with the relative changes in cell size. The changes in cell size ($\Delta S/S$) also influence the fluorescence arising from roGFP2 as can be seen in the upper panel of Figure 4d and Figure S-5d. When I_{488}^{Ox} and I_{488}^{Red} (measured during calibration) are divided by I_{561} at each time point, clear steady state values of the ratios $\hat{I}_{488}^{Ox}$ and $\hat{I}_{488}^{Red}$ are obtained making calibration possible.

Of course, in investigations that do not involve such stressful conditions, changes in cell morphology may not be a problem and the internal standard may not be necessary. Also, it is often sufficient to just report the ratiometric signal $R_{405/488}$, which is immune to the volume changes. But volume changes have been seen by others during OGD. Fekete et al.[71] saw significant swelling/volume changes in acute hippocampus slices during OGD. In an attempt to determine the fluorescence signal from the fluorescent product of the ROS-reactive dye dihydrodichlorofluorescein, they used calcein AM (ROS insensitive) to correct for the changing volume. In our case, it was more appropriate to use cotransfection in order to make measurements on single pyramidal neurons in the CA1 region. Introducing tdTomato as an internal standard allowed us to quantify the degree of oxidation of the sensor over time, $OxD_{roGFP2}(t)$, from the ratiometric signal $I_{405}/I_{488}(t)$. OxD_{roGFP2} is defined as the ratio of the moles of oxidized roGFP2 to the total moles of roGFP2. With assumptions about the local pH, this in turn can be used to infer E_{GSH}. We have applied this method to the determination of changes in OxD_{roGFP2} in the cytoplasm and mitochondria of pyramidal neurons in the CA1 region of the OHSCs as described below.

Quantitative Analysis of Redox Changes in the GSH system in mitochondria and Cytoplasm during OGD/RP. Based on the use of the tdTomato internal standard, we calculated the thermodynamic (equilibrium) quantities related to the GSH/GSSG system in HeLa cells because of their ubiquity in cell biology and in OHSC CA1 pyramidal neurons. We found that $OxD_{roGFP2} = 0.24 \pm 0.05$ (mean ± SEM, $n = 6$) in the mitochondria of HeLa cells under normal conditions. This is indistinguishable within statistical limits from the value of approximately 0.22 from rxYFP Western blot data.[72] In CA1 pyramidal neuronal mitochondrial, OxD_{roGFP2} is 0.30 ± 0.03 (mean ± SEM, $n = 6$). Under resting conditions, we also found that the cytoplasmic values of OxD_{roGFP2} for pyramidal neurons and HeLa cells were 0.07 ± 0.03 and 0.13 ± 0.02, respectively (mean ± SEM, $n = 6$). The degree of oxidation of the GSH/GSSG system, OxD_{GSH}, is the ratio of the moles of oxidized GSH to the total moles of GSH: 2[GSSG]/(2[GSSG] + [GSH]). This cannot be determined accurately without knowing separately the mitochondrial and cytoplasmic total concentrations of GSH: 2[GSSG] + [GSH], which we do not know. However, with a reasonable assumption about the total

DOI: 10.1021/acschemneuro.5b00186
ACS Chem. Neurosci. 2015, 6, 1838−1848

GSH concentrations, all of these values correspond to a degree of oxidation of the GSH/GSSG couple that is less than 0.01.[73]

Figure 5 shows the time-dependent changes in the GSH system in cytoplasm and mitochondria of single pyramidal neurons in the CA1 subfield of OHSCs during OGD/RP. Steady-state values of the Grx1−roGFP2 signal and derived quantities are averages of the last 5 min of each period. The data for pyramidal cells in CA1 (Figure 5) show that the sensor in mitochondria is more oxidized than that in cytoplasm under normal conditions. (OxD_{roGFP2} mito/cyto, 0.30 ± 0.03/0.13 ± 0.02), but E_{GSH} in mitochondria is more negative than that in cytoplasm (mito/cyto, − 351 ± 2/−305 ± 3 mV) because of the different pH values in mitochondria vs cytoplasm (eqs S6 and S7, Supporting Information). Mitochondrial GSH is notably reduced during OGD and then oxidized to a larger extent in RP than control (OxD_{roGFP2}: control/OGD/RP, 0.30 ± 0.03/0.10 ± 0.02/0.45 ± 0.00), whereas no significant change is observed in cytoplasmic GSH (OxD_{roGFP2}: control/OGD/RP, 0.13 ± 0.02/0.16 ± 0.04/0.16 ± 0.03).

We are not aware of ways to determine the redox status of the GSH system in real time other than by using protein-based sensors.[73] Of course, the GSH system's status is in part controlled by ROS, so it is appropriate to consider methods for ROS measurement briefly. There are small-molecule fluorescence approaches to the determination of ROS such as the use of hydroethidine (HEt) and dihydrodichlorofluorescein. They can provide time-dependent information during OGD/RP;[53,71,74] however their selectivity has been questioned.[43,44,46] In addition, these sensors are integrating sensors, so their fluorescence should only increase. Yet often the fluorescence decreases because of photobleaching, export from cells, and swelling.[53,71] The redox-sensitive GFPs, roGFP1 and roGFP2, respond to a variety of oxidants[48] and thus have been applied to record ROS changes in plant root,[51] HeLa cells,[75] hippocampal neurons,[53] chicken cardiomyocytes,[76] mouse liver cell,[77] and rat vascular muscle cells.[78] These protein based sensors reacted broadly to ROS and rather slowly.[51,53,75−79] The creation of the chimeric Grx1−roGFP2 used here has improved the selectivity and response time for seeing changes in the GSH system.

Figure 5 shows that the mitochondrial GSH system becomes more reducing during OGD and more oxidizing during RP in comparison to the pre-OGD control conditions. On the other hand, the cytoplasmic GSH system did not respond to OGD/RP. Abramov et al. recently did a careful investigation of ROS generation during OGD/RP in hippocampal neuron/glia primary cocultures.[74] They found three sources of ROS occurring in series based on MitoSOX and ethidium fluorescence following application of HEt. In the first 10−20 min of OGD, ROS production is mitochondrial and correlated with the presence of inner mitochondrial membrane (IMM) depolarization. After about 25 min (longer than our OGD period), Abramov et al. found that there is a phase during which ROS are produced in the cytoplasm by the xanthine/xanthine oxidase system.[74] During RP, ROS generation occurs in the cytoplasm from the NAD(P)H oxidase system. We observed that the mitochondrial GSH system becomes more reduced quite rapidly at the onset of OGD and that this more reducing status is maintained during OGD. A negative shift in E_{roGFP2} could be caused by a number of factors, for example, import of GSH from cytoplasm,[80] reduction of mitochondrial GSSG, or indeed an increase in local pH. We note that Abramov et al.[74] in primary cultures and others on OHSCs[81−83] have seen rapid IMM depolarization during

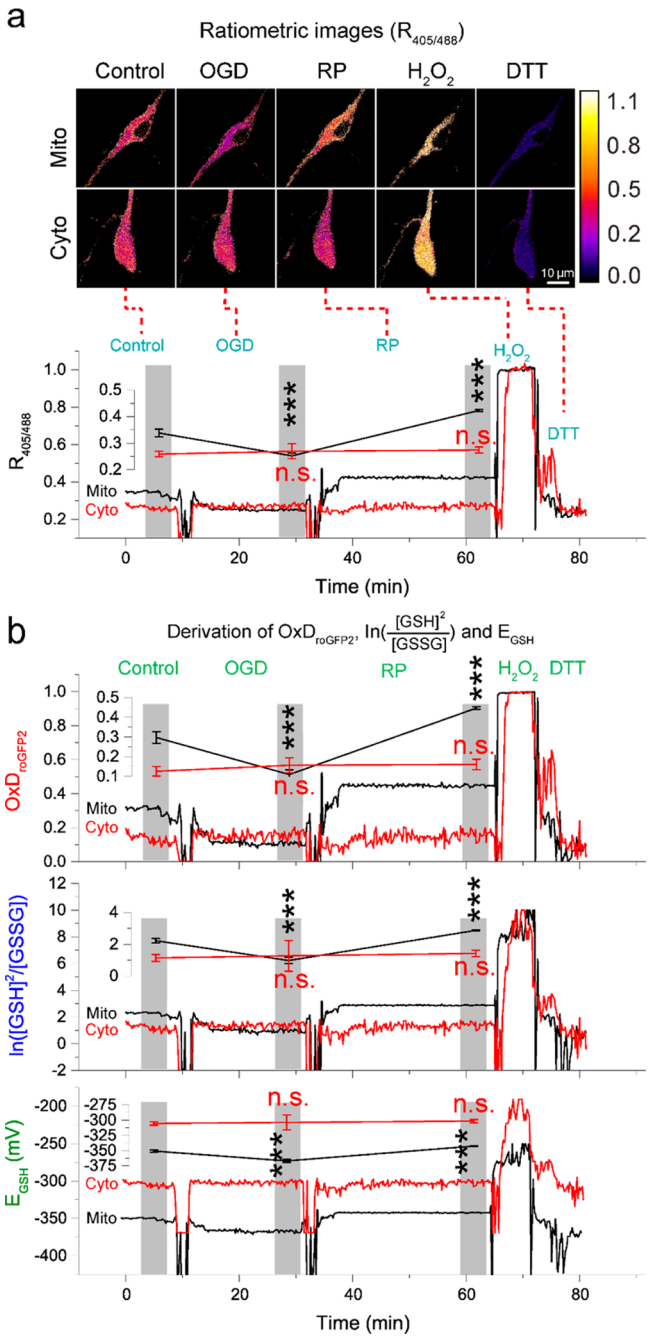

Figure 5. Quantitative analysis of GSH redox changes during OGD/RP. Superfusion system [O+V] described in Figure 1 is used. (a) Ratiometric images of Grx1−roGFP2 in mitochondria (mito) and cytoplasm (cyto) at different points in the OGD/RP procedure. (b) Mitochondria (data shown in black) show a different response during OGD/RP than cytoplasm (data shown in red). Real time data traces are represented. The data in the last 5 min of each condition (indicated by the gray bar) from the traces are averaged and plotted with error bars. The data are compared with the control data (ns, no significant difference, $p > 0.05$; ***$p < 0.001$, $n = 30$ data points, ANOVA). All terms used are defined in eqs S2−S7 in Supporting Information. The curves shown here are representative examples from five sets of measurements on five different OHSCs.

OGD. This would *decrease* the local pH in the matrix. Thus, we can be reasonably sure that the response of mito-Grx1−roGFP2 during OGD represents an increase in the ratio $[GSH]^2/[GSSG]$. That is, the GSH system becomes more

DOI: 10.1021/acschemneuro.5b00186
ACS Chem. Neurosci. 2015, 6, 1838−1848

reduced. Recall that in primary cultures Abramov et al.[74] see a significant increase ROS during OGD, which seems in a sense inconsistent with our observations on GSH. Funke et al.[53] compared the responses of roGFP1 (i.e., the cytoplasm-resident redox responsive GFP with no Grx1) and HEt in primary cultures of hippocampal neurons and glia under various treatments. Indeed, while several treatments led to qualitatively equivalent responses from each sensor, that is, both indicating more oxidizing conditions or more reducing conditions, exposure to glutamate and (separately) uncoupling with carbonyl cyanide 4-(trifluoromethoxy)phenylhydrazone (FCCP) showed opposite responses, more ethidium fluorescence but a more reduced roGFP. In this same work, a 5 min exposure to anoxia led to the same gross changes in roGFP response as we observed though on a much slower time scale. Thus, we are in qualitative agreement with Funke et al., who used the slower, less selective, cytoplasm-resident roGFP1. We conclude that the difference in the ethidium response seen by Abramov et al. and what we have detected during OGD is not likely due a technical issue. While certainly more work is required to understand the contrasting observations, the response of Grx1−roGFP2 may be dominated by increased reducing power during brief OGD rather than by the more oxidizing environment due to excess ROS. There are two contributions to increased reducing power. One is that the pH change from about 8 to about 7 as a result of IMM depolarization increases the difference in redox potentials of the $NADP^+$/NADPH and the GSH systems making the reduction of GSSG by NADPH more thermodynamically favorable (see Supporting Information). In addition, the abundance of NADH from the absence of oxidative phosphorylation can lead to more NADPH production by transhydrogenase[84,85] and thus more GSH from GSSG.

During RP, we find a sharp change in the mitochondrial sensor to more oxidizing potentials. Abramov et al.[74] see an increase in HEt fluorescence as well. This is consistent with the discussion above: the supply of reducing equivalents ultimately derived from fuel and then becoming NADH is a significant factor in mitochondrial GSH status. In the early stages of OGD, without oxygen present, the mitochondrial matrix concentration of NADH should be relatively high, and during RP with the reintroduction of oxygen, it should drop. Thus, the supply of NADPH for acting to reduce GSSG to GSH via glutathione reductase may dictate, at least qualitatively, the GSH system's status.

It is surprising not to find changes in cytoplasmic GSH during OGD/RP. Perhaps cytoplasmic GSH, which has a much larger antioxidant capacity than the mitochondrial GSH system,[74,86] can maintain homeostasis when facing increases in ROS generation in the mitochondria or the cytoplasm.[74] It might be also reasonable to attribute the lack of response in the cytoplasmic GSH system during OGD/RP to the absence of cytoplasmic ROS. According to Abramov et al.,[74] the cytoplasmic sources do not emerge until 25 min of OGD, while our OGD time frame is only 20 min. But H_2O_2 is membrane permeable, so peroxide formed in mitochondria will find its way to the cytoplasm readily. While cytoplasmic generation of ROS may not occur on the 20 min time scale, we would expect the existence of peroxide in the cytoplasm if it is generated in mitochondria. On the other hand, during RP, we would expect to see changes in the cytoplasmic GSH system if indeed superoxide is being formed from NAD(P)H oxidase.[74]

In summary, in order to report OxD_{roGFP2} and E_{GSH} in tissue cultures during OGD/RP, we optimized the OGD/RP protocol in several important ways. (1) We improved the delivery of oxygen and glucose to the tissue cultures so that the time scale of the changes reflect those found *in vivo*. (2) We optimized the transfection protocol to yield neurons expressing the Grx1−roGFP2 in a narrow range of depths in OHSCs. The chosen range of depths corresponds to a range in which changes in pO_2 are reproducible. (3) Deriving OxD_{roGFP2} and E_{GSH} requires a redox insensitive marker to act as a reference intensity during the calibration process following OGD/RP. We introduced tdTomato, a redox insensitive fluorescent protein, specifically to eliminate the apparent effect of changes in cell size on the fluorescent signal of Grx1−roGFP2. Using this optimized protocol, we found that the time dependence of the redox status of the GSH system provides new and perhaps complementary information to that obtained by more classical fluorescence-based techniques. During nonlethal OGD/RP, single CA1 pyramidal neurons show rapid changes in the GSH system in mitochondria. The mitochondria become more reducing during OGD and more oxidizing during RP. The status of the GSH system is dictated by the rates of GSH and GSSG creation and removal. It is possible that changes in the supply of reducing equivalents, not the supply of oxidizing equivalents, that is, ROS, is the dominant factor determining the redox status of the GSH system during OGD/RP. This method could be broadly applied to other types of studies, for example, pharmacological investigations of GSH-related enzymes.[87]

METHODS

Superfusion System. OHSC or HeLa cells were placed in a homemade slice chamber and superfused at a flow rate of 4 mL/min driven with a peristaltic pump (Sci-Q 400DM2, Watson-Marlow, Inc. MA). Solution temperature was maintained at 35 °C by an inline solution heater, SH-27B, under the control of temperature controller, TC-324B (Warner Instruments, LLC. CT, USA). Solution was gassed by an OX miniature gas exchange oxygenator (Living Systems Instrumentation, VT, USA) or by direct bubbling. Gas flow was set to 1.5 L/min with an OMA-1 gas flowmeter (Dwyer Instruments, Inc.). Artificial cerebrospinal fluid[88] (ACSF) is 125 mM NaCl, 2.5 mM KCl, 1.25 mM NaH_2PO_4, 25 mM $NaHCO_3$, 1.0 mM $CaCl_2$, 4.0 mM $MgCl_2$, and 10 mM glucose. Modifed ACSF (MACSF) substitutes 10 mM sucrose for 10 mM glucose. The osmolarity of these solutions was between 290 and 300 mOsm. ACSF gassed with 95% O_2/5% CO_2 and MACSF gassed with 95% N_2/5% CO_2 were alternately introduced into the slice chamber during the control period, OGD, and RP as commonly practiced.[89−93] In the [O+V] system (Figure 1a), we aspirate the solution in the slice chamber by vacuum at the time that the peristaltic pump begins drawing solution from a new reservoir (e.g., from control to OGD). The oxygen partial pressure was monitored (Supporting Information) with an oxygen sensor (OX-25, Unisense, Denmark) connected to a potentiostat (LC-4C amperometric detector, BASi, IN, USA) with the working and guard electrodes at −800 mV with respect to the OX-25 built-in reference electrode. The oxygen sensor was calibrated with zero-oxygen solution (0.1 M NaOH + 0.1 M sodium ascorbate) and ACSF saturated with 95% O_2/5% CO_2. There is no difference in the pO_2 measured in MACSF saturated with 95% O_2/5% CO_2 vs that measured in ACSF. The electrode tip was placed in an OHSC at a particular depth with the aid of a micromanipulator (MP-285, Sutter Instruments). Values of pO_2 in tissue were recorded at various depths with the four superfusion procedures as a function of time.

Expression of the Fluorescent Sensor in OHSCs. Organotypic hippocampal slice cultures (OHSCs) were prepared based on a method modified from Gogolla's protocol.[94] OHSCs are harvested

DOI: 10.1021/acschemneuro.5b00186
ACS Chem. Neurosci. 2015, 6, 1838−1848

from postnatal 7-day old Sprague−Dawley rats (Charles River, Pittsburgh). The surgery protocol was approved by the Institutional Animal Care and Use Committee (IACUC) of the University of Pittsburgh. Preparation details are described in Supporting Information. Cells were then transfected with Grx1−roGFP2[52] or tdTomato[70] or both by biolistic transfection[95] or single cell electroporation[96] (Supporting Information).

Imaging. All imaging experiments were carried out on a Leica TCS SP5II broadband confocal microscope. Cells were imaged with an HCX PL FLUOTAR 5× objective lens with N.A. = 0.15 and an HCX APO L U−V−I water immersion 63× objective lens with N.A. = 0.90. Only images taken with the 63× lens were used for quantitative analysis. Grx1−roGFP2 was excited at 405 and 488 nm, and emission was collected in the range of 500−530 nm. The red fluorescent protein (RFP), tdTomato, was excited at 561 nm, and emission was acquired between 580 and 600 nm. Imaging was carried out by alternately exciting at 488, 405, and 561 nm. The Leica confocal microscope was set up to reduce z-direction shifts with an autofocus algorithm and the hyperdynamic detector. Shifts in the $x-y$ plane were corrected by postprocessing (ImageJ Plugin-Template Matching and Slice Alignment[97]). Image series were acquired every ∼8 s. Raw image files were processed by modules in ImageJ (http://imagej.nih.gov/ij/). Slices in the time-lapse videos were realigned using ImageJ Plugin-Template Matching and Slice Alignment[97] before extracting numerical data for 405, 488, and 561 nm signals. Cell area changes in the time-lapse video were measured with built in functions in ImageJ as follows: autothreshold the images to make the cell area distinguishable from its background, then apply the function module "analyze particle" to measure the cell area within the specified threshold range. Ratiometric images in "Fire" false-color were created by ImageJ.[52] Fluorescence data were processed to obtain the ratio $R_{405/488}$, the oxidation degree of Grx1−roGFP2 (OxD_{roGFP2}), the natural logarithm of the ratio ($[GSH]^2/[GSSG]$), and the redox potential of glutathione (E_{GSH}), according to eqs S2−S7, which are derived from equations described by Meyer and Dick[73] and Gutscher et al.[52] (Supporting Information).

Additional Methods. Description of oxygen measurement, cloning of plasmids, cell and OHSC preparation and transfection, characterization of Grx1−roGFP2, calculation of redox information, and OGD/RP experiments are available in Supporting Information.

■ ASSOCIATED CONTENT

Supporting Information

The Supporting Information is available free of charge on the ACS Publications website at DOI: 10.1021/acschemneuro.5b00186.

Oxygen measurements, cloning of plasmids, cell preparation and transfection, OHSC preparation, transfection, and pO_2 depth profile, calculation of redox information and pH effect, OGD/RP experiments, calibration of oxygen sensor in standard solutions, sketch of optimized superfusion system, lipofectamine-aided transfection in HeLa cells, plasmid transfection of CA1 pyramidal cells in OHSCs, tdTomato used as internal standard to correct the calibration signal from Grx1−roGFP2 in HeLa cells, and detailed descriptions of the videos (PDF)

Video of the determination of the depth of a pyramidal cell expressing tdTomato in an OHSC (AVI)

Video of redox changes of Grx1−roGFP2 sensors (AVI)

Video of tdTomato used to diminish the effect of size on imaging(AVI)

■ AUTHOR INFORMATION

Corresponding Author

*E-mail: sweber@pitt.edu. Phone: 412-624-8520.

Funding

This work was supported by the NIH through Grant R01 GM066018.

Notes

The authors declare no competing financial interest.

■ ACKNOWLEDGMENTS

We thank Dr. Zachary P. Wills (University of Pittsburgh) for technical assistance in gene gun transfection. Jihe Liu (University of Pittsburgh) made the plasmid for expressing mito-tdTomato.

■ REFERENCES

(1) McCann, S. K., and Roulston, C. L. (2013) NADPH oxidase as a therapeutic target for neuroprotection against ischaemic stroke: future perspectives. *Brain Sci. 3*, 561−598.

(2) Kim, J. Y., Kawabori, M., and Yenari, M. A. (2014) Innate Inflammatory Responses in Stroke: Mechanisms and Potential Therapeutic Targets. *Curr. Med. Chem. 21*, 2076−2097.

(3) Duval, D., Delaunay-LeFoll, I., Vimard, F., and Gauberti, M. (2013) Neuroprotective effects of N-acetylcysteine: a review. *Brain Res. J. 6*, 309−337.

(4) Cornelius, C., Crupi, R., Calabrese, V., Graziano, A., Milone, P., Pennisi, G., Radak, Z., Calabrese, E. J., and Cuzzocrea, S. (2013) Traumatic Brain Injury: Oxidative Stress and Neuroprotection. *Antioxid. Redox Signaling 19*, 836−853.

(5) Rodriguez-Rodriguez, A., Egea-Guerrero, J. J., Murillo-Cabezas, F., and Carrillo-Vico, A. (2014) Oxidative Stress in Traumatic Brain Injury. *Curr. Med. Chem. 21*, 1201−1211.

(6) Abdul-Muneer, P. M., Chandra, N., and Haorah, J. (2015) Interactions of Oxidative Stress and Neurovascular Inflammation in the Pathogenesis of Traumatic Brain Injury. *Mol. Neurobiol. 51*, 966.

(7) Larson, J., Drew, K. L., Folkow, L. P., Milton, S. L., and Park, T. J. (2014) No oxygen? No problem! intrinsic brain tolerance to hypoxia in vertebrates. *J. Exp. Biol. 217*, 1024−1039.

(8) Lasierra-Cirujeda, J., Coronel, P., Aza, M. J., and Gimeno, M. (2013) Beta-amyloidolysis and glutathione in Alzheimer's disease. *J. Blood Med. 4*, 31−38.

(9) Aliev, G., Priyadarshini, M., Reddy, V. P., Grieg, N. H., Kaminsky, Y., Cacabelos, R., Ashraf, G. M., Jabir, N. R., Kamal, M. A., Nikolenko, V. N., Zamyatnin, A. A., Jr., Benberin, V. V., and Bachurin, S. O. (2014) Oxidative Stress Mediated Mitochondrial and Vascular Lesions as Markers in the Pathogenesis of Alzheimer Disease. *Curr. Med. Chem. 21*, 2208−2217.

(10) Butterfield, D. A., Di Domenico, F., and Barone, E. (2014) Elevated risk of type 2 diabetes for development of Alzheimer disease: A key role for oxidative stress in brain. *Biochim. Biophys. Acta, Mol. Basis Dis. 1842*, 1693−1706.

(11) Schapira, A. H. V. (2008) Mitochondria in the aetiology and pathogenesis of Parkinson's disease. *Lancet Neurol. 7*, 97−109.

(12) Guzman, J. N., Sanchez-Padilla, J., Wokosin, D., Kondapalli, J., Ilijic, E., Schumacker, P. T., and Surmeier, D. J. (2010) Oxidant stress evoked by pacemaking in dopaminergic neurons is attenuated by DJ-1. *Nature 468*, 696−700.

(13) Muller, M., and Leavitt, B. R. (2014) Iron dysregulation in Huntington's disease. *J. Neurochem. 130*, 328−350.

(14) Gil-Mohapel, J., Brocardo, P. S., and Christie, B. R. (2014) The Role of Oxidative Stress in Huntington's Disease: Are Antioxidants Good Therapeutic Candidates? *Curr. Drug Targets 15*, 454−468.

(15) Pandya, C. D., Howell, K. R., and Pillai, A. (2013) Antioxidants as potential therapeutics for neuropsychiatric disorders. *Prog. Neuro-Psychopharmacol. Biol. Psychiatry 46*, 214−223.

(16) Xu, Y., Wang, C., Klabnik, J. J., and O'Donnell, J. M. (2014) Novel Therapeutic Targets in Depression and Anxiety: Antioxidants as a Candidate Treatment. *Curr. Neuropharmacol. 12*, 108−119.

(17) Hassan, W., Silva, C. E. B., Mohammadzai, I. U., Teixeira da Rocha, J. B., and Landeira-Fernandez, J. (2014) Association of

DOI: 10.1021/acschemneuro.5b00186
ACS Chem. Neurosci. 2015, 6, 1838−1848

Oxidative Stress to the Genesis of Anxiety: Implications for Possible Therapeutic Interventions. *Curr. Neuropharmacol. 12*, 120−139.
(18) D'Amico, E., Factor-Litvak, P., Santella, R. M., and Mitsumoto, H. (2013) Clinical perspective on oxidative stress in sporadic amyotrophic lateral sclerosis. *Free Radical Biol. Med. 65*, 509−527.
(19) Chan, S. H. H., and Chan, J. Y. H. (2014) Brain Stem NOS and ROS in Neural Mechanisms of Hypertension. *Antioxid. Redox Signaling 20*, 146−163.
(20) Colamartino, M., Padua, L., Cornetta, T., Testa, A., and Cozzi, R. (2012) Recent advances in pharmacological therapy of Parkinson's disease: levodopa and carbidopa protective effects against DNA oxidative damage. *Health 4*, 1191−1199.
(21) Mari, M., Morales, A., Colell, A., Garcia-Ruiz, C., Kaplowitz, N., and Fernandez-Checa, J. C. (2013) Mitochondrial glutathione: Features, regulation and role in disease. *Biochim. Biophys. Acta, Gen. Subj. 1830*, 3317−3328.
(22) Kembro, J. M., Aon, M. A., Winslow, R. L., O'Rourke, B., and Cortassa, S. (2013) Integrating Mitochondrial Energetics, Redox and ROS Metabolic Networks: A Two-Compartment Model. *Biophys. J. 104*, 332−343.
(23) Niatsetskaya, Z. V., Sosunov, S. A., Matsiukevich, D., Utkina-Sosunova, I. V., Ratner, V. I., Starkov, A. A., and Ten, V. S. (2012) The oxygen free radicals originating from mitochondrial complex I contribute to oxidative brain injury following hypoxia-ischemia in neonatal mice. *J. Neurosci. 32*, 3235−3244.
(24) Finkel, T. (2011) Signal transduction by reactive oxygen species. *J. Cell Biol. 194*, 7−15.
(25) Patel, J. C., and Rice, M. E. (2012) Classification of H2O2 as a Neuromodulator that Regulates Striatal Dopamine Release on a Subsecond Time Scale. *ACS Chem. Neurosci. 3*, 991−1001.
(26) Rice, M. E. (2011) H2O2: a dynamic neuromodulator. *Neuroscientist 17*, 389−406.
(27) Bao, L., Avshalumov, M. V., Patel, J. C., Lee, C. R., Miller, E. W., Chang, C. J., and Rice, M. E. (2009) Mitochondria are the source of hydrogen peroxide for dynamic brain-cell signaling. *J. Neurosci. 29*, 9002−9010.
(28) Waypa, G. B., Marks, J. D., Guzy, R. D., Mungai, P. T., Schriewer, J. M., Dokic, D., Ball, M. K., and Schumacker, P. T. (2013) Superoxide generated at mitochondrial complex III triggers acute responses to hypoxia in the pulmonary circulation. *Am. J. Respir. Crit. Care Med. 187*, 424−432.
(29) Mungai, P. T., Waypa, G. B., Jairaman, A., Prakriya, M., Dokic, D., Ball, M. K., and Schumacker, P. T. (2011) Hypoxia triggers AMPK activation through reactive oxygen species-mediated activation of calcium release-activated calcium channels. *Mol. Cell. Biol. 31*, 3531−3545.
(30) Currais, A., and Maher, P. (2013) Functional Consequences of Age-Dependent Changes in Glutathione Status in the Brain. *Antioxid. Redox Signaling 19*, 813−822.
(31) Kudin, A. P., Augustynek, B., Lehmann, A. K., Kovács, R., and Kunz, W. S. (2012) The contribution of thioredoxin-2 reductase and glutathione peroxidase to H2O2 detoxification of rat brain mitochondria. *Biochim. Biophys. Acta, Bioenerg. 1817*, 1901−1906.
(32) Gu, F., Chauhan, V., and Chauhan, A. (2013) Impaired synthesis and antioxidant defense of glutathione in the cerebellum of autistic subjects: Alterations in the activities and protein expression of glutathione-related enzymes. *Free Radical Biol. Med. 65*, 488−496.
(33) Pocernich, C. B., and Butterfield, D. A. (2012) Elevation of glutathione as a therapeutic strategy in Alzheimer disease. *Biochim. Biophys. Acta, Mol. Basis Dis. 1822*, 625−630.
(34) Smeyne, M., and Smeyne, R. J. (2013) Glutathione metabolism and Parkinson's disease. *Free Radical Biol. Med. 62*, 13−25.
(35) Rose, S., Melnyk, S., Pavliv, O., Bai, S., Nick, T. G., Frye, R. E., and James, S. J. (2012) Evidence of oxidative damage and inflammation associated with low glutathione redox status in the autism brain. *Transl. Psychiatry 2*, e134.
(36) Herdegen, T., and Leah, J. D. (1998) Inducible and constitutive transcription factors in the mammalian nervous system: control of gene expression by Jun, Fos and Krox, and CREB/ATF proteins. *Brain Res. Rev. 28*, 370−490.
(37) Cheng, Y., Deshmukh, M., D'Costa, A., Demaro, J. A., Gidday, J. M., Shah, A., Sun, Y., Jacquin, M. F., Johnson, E. M., Jr., and Holtzman, D. M. (1998) Caspase inhibitor affords neuroprotection with delayed administration in a rat model of neonatal hypoxic-ischemic brain injury. *J. Clin. Invest. 101*, 1992−1999.
(38) Banasiak, K. J., Xia, Y., and Haddad, G. G. (2000) Mechanisms underlying hypoxia-induced neuronal apoptosis. *Prog. Neurobiol. (Oxford, U. K.) 62*, 215−249.
(39) Crespi, F. (2014) Hydrogen peroxide monitored in vivo, in situ and in real time in rat brain, is it a marker of central cholinergic dynamics? *Anal. Methods 6*, 1174−1181.
(40) Roberts, J. G., Toups, J. V., Eyualem, E., McCarty, G. S., and Sombers, L. A. (2013) In Situ Electrode Calibration Strategy for Voltammetric Measurements In Vivo. *Anal. Chem. (Washington, DC, U. S.) 85*, 11568−11575.
(41) Ross, A. E., and Venton, B. J. (2014) Sawhorse Waveform Voltammetry for Selective Detection of Adenosine, ATP, and Hydrogen Peroxide. *Anal. Chem. (Washington, DC, U. S.) 86*, 7486−7493.
(42) Sanford, A. L., Morton, S. W., Whitehouse, K. L., Oara, H. M., Lugo-Morales, L. Z., Roberts, J. G., and Sombers, L. A. (2010) Voltammetric Detection of Hydrogen Peroxide at Carbon Fiber Microelectrodes. *Anal. Chem. 82*, 5205−5210.
(43) Kalyanaraman, B., Darley-Usmar, V., Davies, K. J. A., Dennery, P. A., Forman, H. J., Grisham, M. B., Mann, G. E., Moore, K., Roberts, L. J., II, and Ischiropoulos, H. (2012) Measuring reactive oxygen and nitrogen species with fluorescent probes: challenges and limitations. *Free Radical Biol. Med. 52*, 1−6.
(44) Karlsson, M., Kurz, T., Brunk, U. T., Nilsson, S. E., and Frennesson, C. I. (2010) What does the commonly used DCF test for oxidative stress really show? *Biochem. J. 428*, 183−190.
(45) Kristiansen, K. A., Jensen, P. E., Møller, I. M., and Schulz, A. (2009) Monitoring reactive oxygen species formation and localisation in living cells by use of the fluorescent probe CM-H(2)DCFDA and confocal laser microscopy. *Physiol. Plant. 136*, 369−383.
(46) Zielonka, J., and Kalyanaraman, B. (2010) Hydroethidine- and MitoSOX-derived red fluorescence is not a reliable indicator of intracellular superoxide formation: Another inconvenient truth. *Free Radical Biol. Med. 48*, 983−1001.
(47) Ostergaard, H., Tachibana, C., and Winther, J. R. (2004) Monitoring disulfide bond formation in the eukaryotic cytosol. *J. Cell Biol. 166*, 337−345.
(48) Dooley, C. T., Dore, T. M., Hanson, G. T., Jackson, W. C., Remington, S. J., and Tsien, R. Y. (2004) Imaging Dynamic Redox Changes in Mammalian Cells with Green Fluorescent Protein Indicators. *J. Biol. Chem. 279*, 22284−22293.
(49) Hanson, G. T., Aggeler, R., Oglesbee, D., Cannon, M., Capaldi, R. A., Tsien, R. Y., and Remington, S. J. (2004) Investigating Mitochondrial Redox Potential with Redox-sensitive Green Fluorescent Protein Indicators. *J. Biol. Chem. 279*, 13044−13053.
(50) Cannon, M. B., and Remington, S. J. (2006) Re-engineering redox-sensitive green fluorescent protein for improved response rate. *Protein Sci. 15*, 45−57.
(51) Meyer, A. J., Brach, T., Marty, L., Kreye, S., Rouhier, N., Jacquot, J.-P., and Hell, R. (2007) Redox-sensitive GFP in Arabidopsis thaliana is a quantitative biosensor for the redox potential of the cellular glutathione redox buffer. *Plant J. 52*, 973−986.
(52) Gutscher, M., Pauleau, A.-L., Marty, L., Brach, T., Wabnitz, G. H., Samstag, Y., Meyer, A. J., and Dick, T. P. (2008) Real-time imaging of the intracellular glutathione redox potential. *Nat. Methods 5*, 553−559.
(53) Funke, F., Gerich, F. J., and Müller, M. (2011) Dynamic, semi-quantitative imaging of intracellular ROS levels and redox status in rat hippocampal neurons. *NeuroImage 54*, 2590−2602.
(54) Grosser, E., Hirt, U., Janc, O. A., Menzfeld, C., Fischer, M., Kempkes, B., Vogelgesang, S., Manzke, T. U., Opitz, L., Salinas-Riester, G., and Mueller, M. (2012) Oxidative burden and mitochondrial

DOI: 10.1021/acschemneuro.5b00186
ACS Chem. Neurosci. 2015, 6, 1838−1848

dysfunction in a mouse model of Rett syndrome. *Neurobiol. Dis. 48*, 102−114.
(55) Hasel, P., McKay, S., Qiu, J., and Hardingham, G. E. (2015) Selective dendritic susceptibility to bioenergetic, excitotoxic and redox perturbations in cortical neurons. *Biochim. Biophys. Acta, Mol. Cell Res. 1853*, 2066.
(56) Breckwoldt, M. O., Pfister, F. M. J., Bradley, P. M., Marinkovic, P., Williams, P. R., Brill, M. S., Plomer, B., Schmalz, A., St Clair, D. K., Naumann, R., Griesbeck, O., Schwarzlander, M., Godinho, L., Bareyre, F. M., Dick, T. P., Kerschensteiner, M., and Misgeld, T. (2014) Multiparametric optical analysis of mitochondrial redox signals during neuronal physiology and pathology in vivo. *Nat. Med. 20*, 555.
(57) Stoppini, L., Buchs, P. A., and Muller, D. (1991) A simple method for organotypic cultures of nervous tissue. *J. Neurosci. Methods 37*, 173−182.
(58) Laake, J. H., Haug, F. M., Wieloch, T., and Ottersen, O. P. (1999) A simple in vitro model of ischemia based on hippocampal slice cultures and propidium iodide fluorescence. *Brain Res. Protoc. 4*, 173−184.
(59) Ahlgren, H., Henjum, K., Ottersen, O. P., and Runden-Pran, E. (2011) Validation of organotypical hippocampal slice cultures as an ex vivo model of brain ischemia: Different roles of NMDA receptors in cell death signalling after exposure to NMDA or oxygen and glucose deprivation. *Cell Tissue Res. 345*, 329−341.
(60) Noraberg, J., Poulsen, F. R., Blaabjerg, M., Kristensen, B. W., Bonde, C., Montero, M., Meyer, M., Gramsbergen, J. B., and Zimmer, J. (2005) Organotypic hippocampal slice cultures for studies of brain damage, neuroprotection and neurorepair. *Curr. Drug Targets: CNS Neurol. Disord. 4*, 435−452.
(61) Guy, Y., Rupert, A. E., Sandberg, M., and Weber, S. G. (2011) A simple method for measuring organotypic tissue slice culture thickness. *J. Neurosci. Methods 199*, 78−81.
(62) Huchzermeyer, C., Berndt, N., Holzhutter, H.-G., and Kann, O. (2013) Oxygen consumption rates during three different neuronal activity states in the hippocampal CA3 network. *J. Cereb. Blood Flow Metab. 33*, 263−271.
(63) Sacco, R. L., Kasner, S. E., Broderick, J. P., Caplan, L. R., Connors, J. J., Culebras, A., Elkind, M. S. V., George, M. G., Hamdan, A. D., Higashida, R. T., Hoh, B. L., Janis, L. S., Kase, C. S., Kleindorfer, D. O., Lee, J.-M., Moseley, M. E., Peterson, E. D., Turan, T. N., Valderrama, A. L., and Vinters, H. V. (2013) An Updated Definition of Stroke for the 21st Century: A Statement for Healthcare Professionals From the American Heart Association/American Stroke Association. *Stroke 44*, 2064−2089.
(64) Pundik, S., Xu, K., and Sundararajan, S. (2012) Reperfusion brain injury: Focus on cellular bioenergetics. *Neurology 79*, S44−S51.
(65) Nakai, A., Kuroda, S., Kristián, T., and Siesjö, B. K. (1997) The Immunosuppressant Drug FK506 Ameliorates Secondary Mitochondrial Dysfunction Following Transient Focal Cerebral Ischemia in the Rat. *Neurobiol. Dis. 4*, 288−300.
(66) Peters, O., Back, T., Lindauer, U., Busch, C., Megow, D., Dreier, J., and Dirnagl, U. (1998) Increased Formation of Reactive Oxygen Species After Permanent and Reversible Middle Cerebral Artery Occlusion in the Rat. *J. Cereb. Blood Flow Metab. 18*, 196−205.
(67) Okada, T., Teranishi, K., Chen, Y., Tomori, T., Strasser, A., Lenz, F., McCarron, R., and Spatz, M. (2012) Reversal of Postischemic Hypoperfusion by Tempol: Endothelial Signal Transduction Mechanism. *Neurochem. Res. 37*, 680−688.
(68) Westermaier, T., Jauss, A., Eriskat, J., Kunze, E., and Roosen, K. (2009) Time-course of cerebral perfusion and tissue oxygenation in the first 6[thinsp]h after experimental subarachnoid hemorrhage in rats. *J. Cereb. Blood Flow Metab. 29*, 771−779.
(69) Prunell, G. F., Mathiesen, T., and Svendgaard, N.-A. (2004) Experimental subarachnoid hemorrhage: cerebral blood flow and brain metabolism during the acute phase in three different models in the rat. *Neurosurgery 54*, 426−436.
(70) Shaner, N. C., Campbell, R. E., Steinbach, P. A., Giepmans, B. N. G., Palmer, A. E., and Tsien, R. Y. (2004) Improved monomeric red, orange and yellow fluorescent proteins derived from Discosoma sp. red fluorescent protein. *Nat. Biotechnol. 22*, 1567−1572.
(71) Fekete, A., Vizi, E. S., Kovacs, K. J., Lendvai, B., and Zelles, T. (2008) Layer-specific differences in reactive oxygen species levels after oxygen-glucose deprivation in acute hippocampal slices. *Free Radical Biol. Med. 44*, 1010−1022.
(72) Banach-Latapy, A., He, T., Dardalhon, M., Vernis, L., Chanet, R., and Huang, M.-E. (2013) Redox-sensitive YFP sensors for monitoring dynamic compartment-specific glutathione redox state. *Free Radical Biol. Med. 65*, 436−445.
(73) Meyer, A. J., and Dick, T. P. (2010) Fluorescent Protein-Based Redox Probes. *Antioxid. Redox Signaling 13*, 621−650.
(74) Abramov, A. Y., Scorziello, A., and Duchen, M. R. (2007) Three Distinct Mechanisms Generate Oxygen Free Radicals in Neurons and Contribute to Cell Death during Anoxia and Reoxygenation. *J. Neurosci. 27*, 1129−1138.
(75) Dooley, C. T., Dore, T. M., Hanson, G. T., Jackson, W. C., Remington, S. J., and Tsien, R. Y. (2004) Imaging dynamic redox changes in mammalian cells with green fluorescent protein indicators. *J. Biol. Chem. 279*, 22284−22293.
(76) Robin, E., Guzy, R. D., Loor, G., Iwase, H., Waypa, G. B., Marks, J. D., Hoek, T. L. V., and Schumacker, P. T. (2007) Oxidant Stress during Simulated Ischemia Primes Cardiomyocytes for Cell Death during Reperfusion. *J. Biol. Chem. 282*, 19133−19143.
(77) Haga, S., Remington, S. J., Morita, N., Terui, K., and Ozaki, M. (2009) Hepatic Ischemia Induced Immediate Oxidative Stress after Reperfusion and Determined the Severity of the Reperfusion-Induced Damage. *Antioxid. Redox Signaling 11*, 2563−2572.
(78) Waypa, G. B., Marks, J. D., Guzy, R., Mungai, P. T., Schriewer, J., Dokic, D., and Schumacker, P. T. (2010) Hypoxia Triggers Subcellular Compartmental Redox Signaling in Vascular Smooth Muscle Cells. *Circ. Res. 106*, 526−535.
(79) Lukyanov, K. A., and Belousov, V. V. (2014) Genetically encoded fluorescent redox sensors. *Biochim. Biophys. Acta, Gen. Subj. 1840*, 745−756.
(80) Lash, L. H. (2006) Mitochondrial glutathione transport: Physiological, pathological and toxicological implications. *Chem.-Biol. Interact. 163*, 54−67.
(81) Gerich, F. J., Hepp, S., Probst, I., and Muller, M. (2006) Mitochondrial inhibition prior to oxygen-withdrawal facilitates the occurrence of hypoxia-induced spreading depression in rat hippocampal slices. *J. Neurophysiol. 96*, 492−504.
(82) Bahar, S., Fayuk, D., Somjen, G. G., Aitken, P. G., and Turner, D. A. (2000) Mitochondrial and Intrinsic Optical Signals Imaged During Hypoxia and Spreading Depression in Rat Hippocampal Slices. *J. Neurophysiol. 84*, 311−324.
(83) Schuchmann, S., Lückermann, M., Kulik, A., Heinemann, U., and Ballanyi, K. (2000) Ca2+- and Metabolism-Related Changes of Mitochondrial Potential in Voltage-Clamped CA1 Pyramidal Neurons In Situ. *J. Neurophysiol. 83*, 1710−1721.
(84) Vogel, R., Wiesinger, H., Hamprecht, B., and Dringen, R. (1999) The regeneration of reduced glutathione in rat forebrain mitochondria identifies metabolic pathways providing the NADPH required. *Neurosci. Lett. 275*, 97−100.
(85) Andreyev, A. Y., Kushnareva, Y. E., Murphy, A. N., and Starkov, A. A. (2015) Mitochondrial ROS metabolism: 10 Years later. *Biochemistry (Moscow) 80*, 517−531.
(86) Marí, M., Morales, A., Colell, A., García-Ruiz, C., and Fernández-Checa, J. C. (2009) Mitochondrial Glutathione, a Key Survival Antioxidant. *Antioxid. Redox Signaling 11*, 2685−2700.
(87) Dringen, R., Pawlowski, P. G., and Hirrlinger, J. (2005) Peroxide detoxification by brain cells. *J. Neurosci. Res. 79*, 157−165.
(88) Galván, E. J., Cosgrove, K. E., Mauna, J. C., Card, J. P., Thiels, E., Meriney, S. D., and Barrionuevo, G. (2010) Critical Involvement of Postsynaptic Protein Kinase Activation in Long-Term Potentiation at Hippocampal Mossy Fiber Synapses on CA3 Interneurons. *J. Neurosci. 30*, 2844−2855.
(89) Alluri, H., Anasooya Shaji, C., Davis, M. L., and Tharakan, B. (2015) Oxygen-Glucose Deprivation and Reoxygenation as an In Vitro

DOI: 10.1021/acschemneuro.5b00186
ACS Chem. Neurosci. 2015, 6, 1838−1848

Ischemia-Reperfusion Injury Model for Studying Blood-Brain Barrier Dysfunction. *J. Visualized Exp.*, e52699.
(90) Fontella, F. U., Cimarosti, H., Crema, L. M., Thomazi, A. P., Leite, M. C., Salbego, C., Gonçalves, C. A. S., Wofchuk, S., Dalmaz, C., and Netto, C. A. (2005) Acute and repeated restraint stress influences cellular damage in rat hippocampal slices exposed to oxygen and glucose deprivation. *Brain Res. Bull. 65*, 443−450.
(91) Jarvis, C. R., Anderson, T. R., and Andrew, R. D. (2001) Anoxic Depolarization Mediates Acute Damage Independent of Glutamate in Neocortical Brain Slices. *Cerebral Cortex 11*, 249−259.
(92) Obeidat, A. S., Jarvis, C. R., and Andrew, R. D. (2000) Glutamate Does Not Mediate Acute Neuronal Damage After Spreading Depression Induced By O2/Glucose Deprivation in the Hippocampal Slice. *J. Cereb. Blood Flow Metab. 20*, 412−422.
(93) Xie, M., Wang, W., Kimelberg, H. K., and Zhou, M. (2008) Oxygen and glucose deprivation-induced changes in astrocyte membrane potential and their underlying mechanisms in acute rat hippocampal slices. *J. Cereb. Blood Flow Metab. 28*, 456−467.
(94) Gogolla, N., Galimberti, I., DePaola, V., and Caroni, P. (2006) Preparation of organotypic hippocampal slice cultures for long-term live imaging. *Nat. Protoc. 1*, 1165−1171.
(95) Woods, G., and Zito, K. (2008) Preparation of Gene Gun Bullets and Biolistic Transfection of Neurons in Slice Culture. *J. Visualized Exp.*, e675.
(96) Haas, K., Sin, W.-C., Javaherian, A., Li, Z., and Cline, H. T. (2001) Single-Cell Electroporationfor Gene Transfer In Vivo. *Neuron 29*, 583−591.
(97) Tseng, Q., Duchemin-Pelletier, E., Deshiere, A., Balland, M., Guillou, H., Filhol, O., and Théry, M. (2012) Spatial organization of the extracellular matrix regulates cell−cell junction positioning. *Proc. Natl. Acad. Sci. U. S. A. 109*, 1506−1511.

DOI: 10.1021/acschemneuro.5b00186
ACS Chem. Neurosci. 2015, 6, 1838−1848